Parkinsonism and Related Disorders 63 (2019) 106–110

Contents lists available at ScienceDirect

Parkinsonism and Related Disorders

journal homepage: www.elsevier.com/locate/parkreldis

Speculating the timing of iron deposition in the putamen in multiple system atrophy

Myung Jun Lee[a], Tae-Hyung Kim[b], Seung Joo Kim[c], Chi-Woong Mun[d], Jin-Hong Shin[e], Gha-Hyun Lee[a], Jae-Hyeok Lee[e,*]

[a] Department of Neurology, Pusan National University Hospital, Pusan National University School of Medicine and Biomedical Research Institute, Busan, Republic of Korea
[b] Research Institute for Convergence of Biomedical Science and Technology, Pusan National University Yangsan Hospital, Yangsan, Republic of Korea
[c] Department of Neurology, Samsung Medical Center, Sungkyunkwan University School of Medicine, Seoul, Republic of Korea
[d] Department of Biomedical Engineering, Inje University, Gimhae, Republic of Korea
[e] Department of Neurology, Research Institute for Convergence of Biomedical Science and Technology, Pusan National University Yangsan Hospital, Pusan National University School of Medicine, Yangsan, Republic of Korea

ARTICLE INFO

Keywords:
Multiple system atrophy
Magnetic resonance imaging
Multimodal imaging
Conditional probability modeling
Iron deposition

ABSTRACT

Background & objective: Although iron accumulation is thought to be associated with neurodegenerative processes, the timing of putaminal iron deposition during the disease course of multiple system atrophy (MSA) remains unclear. We sought to investigate the temporal pattern of iron deposition in the putamen of MSA patients by calculating the conditional probabilities (CPs) of multimodal MRI changes.
Methods: We simultaneously measured putaminal R2*, volume and MD values of 39 probable MSA patients and 22 control subjects. The presence of significant MRI changes was defined as higher R2* and MD values, or lower volumes than cut-off values derived from mean values in control putamen. The CPs of R2* changes without MD or volume changes were then compared with those of MD or volume changes without R2* changes.
Results: Regardless of the cut-off values, the CPs of R2* increments without MD or volume changes were significantly lower than those for MD or volume changes without R2* increments. The associations of R2* with volume and MD values appeared in non-linear exponential and quadratic patterns, respectively.
Conclusions: Our findings suggest that putaminal iron accumulation would occur under volume atrophy or MD increments. Thus, iron deposition in the putamen of MSA patients is likely a secondary byproduct of neurodegeneration.

1. Introduction

In patients with multiple system atrophy (MSA), putaminal hypointensity on T2-weighted, T2*-weighted or susceptibility-weighted imaging (SWI) presumably reflects pathological iron deposition being unevenly distributed within the putamen and is predominantly observed in the posterior putamen with a posterolateral to anteromedial gradient [1]. This can be useful for differentiating MSA from Parkinson's disease (PD) [2,3], as well as for distinguishing between the parkinsonian (MSA-P) and cerebellar variants (MSA-C) [3,4]. Iron-related signal changes in the putamen of MSA patients are known to be correlated with changes in other MRI parameters, which reflect markers of neurodegeneration such as volume and mean diffusivity (MD) values [2,3].

Although previous MRI studies have shown a correlation between iron-related signal changes with the extent of atrophy and microstructural changes detected by diffusion tensor imaging (DTI), the timing and progression of iron accumulation in the putamen of MSA patients remains unclear [1,3,5]. MSA is a relatively rare neurodegenerative disorder with a rapid disease progression [6]. Thus, there are challenges in conducting prospective cohorts with the inclusion of a sufficient number of early-stage MSA patients to investigate the temporal-causal relationship.

Calculating conditional probabilities (CPs) is a method for determining the likelihood of the occurrence of an event, given that a different event has occurred. Recent postmortem and neuroimaging studies have predicted the sequential order of pathological changes using cross-sectional results [7–9]. Thus, a comparison between CPs of

* Corresponding author. Department of Neurology, Research Institute for Convergence of Biomedical Science and Technology, Pusan National University Yangsan Hospital, Beomo-ri, Mulgum-eup, Yangsan, Gyeongsangnam-do, 626-770, Republic of Korea.
E-mail address: jhlee.neuro@pusan.ac.kr (J.-H. Lee).

https://doi.org/10.1016/j.parkreldis.2019.02.030
Received 26 November 2018; Received in revised form 17 February 2019; Accepted 19 February 2019

multimodal MRI data from MSA patients may be an alternative method for speculating on the timing of iron deposition. In the present study, we investigated the temporal relationship between R2*, volume, and MD values using comparisons of CPs.

2. Methods

2.1. Subjects

We enrolled 39 patients with probable MSA according to international consensus criteria [10] and 22 control subjects from Pusan National University Yangsan Hospital. All patients had at least two-year follow-up period. Of the MSA patients, 25 showed predominant parkinsonian motor deficits (MSA-P) and the remaining 14 patients had predominant cerebellar features (MSA-C). Subjects with vascular lesions or motion artifacts found on brain MRI were excluded. None of the control subjects had a history of head trauma, stroke, or any neurological or psychiatric illnesses. Spinocerebellar ataxia (SCA) 1, 2, 3, 6, 7, 17, and Dentatorubral-pallidoluysian atrophy (DRPLA) were excluded, as MSA-like cerebellar symptoms can be shared by these SCA subtypes. The disease severity of the MSA patients was assessed by Hoehn and Yahr (H&Y) stage, the motor part of the Unified Parkinson's Disease Rating Scale (UPDRS-III), and the Unified Multiple System Atrophy Rating Scale part II (UMSARS-II). All MSA patients had received dopaminergic medications, however, none of them showed significant improvement (> 20% reduction of baseline UPDRS-III). Written informed consent was obtained from all subjects participating in the study, which was approved by the Institutional Review Board of Pusan National University Yangsan Hospital, in accordance with the principles of the Helsinki Declaration.

2.2. MRI acquisition and analyses

All subjects underwent 3T brain MRI (Verio, Siemens, Erlangen, Germany). The axial scans were set parallel to the intercommissural line. The following sequences were performed: T1-weighted magnetization prepared rapid acquisition gradient recalled echo (MPRAGE) pulse sequence [repetition time (TR)/echo time (TE)/inversion time (TI) = 1900/2.2/900 ms, Flip angle (FA) = 9°, 1 mm^3 isotropic voxel size, acquisition time = 5 min 28 s], 3D multi-echo FLASH (fast low angle shot) pulse sequence to acquire R2* images [TR = 24 ms, TE = 2.26/4.91/7.56/10.21/12.86/15.51/18.16/20.81 ms, Flip angle = 6°, and 1 mm^3 isotropic voxel size], and echo-planar diffusion tensor imaging (DTI) to generate mean diffusivity (MD) maps [TR = 5100 ms, TE = 90 ms, flip angle = 90°, NEX (number of average) = 3, b value = 100, 1000s/mm^2, gradient direction = 20, acquisition matrix = 96 * 96, FOV = 220 * 220 mm^2, slice thickness = 2.3 mm, total number of slices = 40, 2.3 mm^3 isotropic voxel size].

R2* maps were calculated by the regression of log signals of the eight multi-echo volumes using customized Matlab tools (The MathWorks Inc., MA, USA). R2* and MD maps were linearly registered to their T1-weighted images using FLIRT (FMRIB's Linear Image Registration Tool). To acquire the R2* values, MD values, and volumes of the putamen, automatic segmentation was performed on the basis of T1-weighted images using FreeSurfer v5.3 (http://surfer.nmr.mgh.harvard.edu/). We verified the accuracy of the ROI segmentation on each subject. Due to considerable left-right asymmetry [11], we analyzed each putamen separately.

2.3. Conditional probabilities of multimodal MRI changes

The theoretical background and details of the CP method for determining the sequential order of two conditions have been described in a previous article [7]. If events are denoted as X and Y, and whether the occurrence of events are symbolized as a plus or minus sign, the CP method compares probabilities of event X without Y (X+|Y-) and those of event Y without X (X-|Y+). The CP method assesses the evidence against the null hypothesis that (X+|Y-) and (X-|Y+) were equally likely and therefore X and Y were part of the same time period. If the CP of (X+|Y-) was significantly higher than that of (X-|Y+), the CP method suggests a possibility that event X would precede the occurrence of event Y. As shown in a previous article [9], we compared CPs using z-test. (Supplementary Material 1).

To define the presence of MRI parameter changes, we used the cut-off values of 1.5, 2.0 or 2.5 SD away from the mean values of control putamen, i.e., "significant MRI parameter change" represents R2* and MD values > cut-off values, or volume < cut-off values.

We obtained unstandardized residuals of multimodal MRI data in both groups using generalized linear model with age and gender as covariate to avoid potential bias from differences in age and gender ratio between MSA and control subjects.

2.4. Statistical analyses

A comparison of continuous variables showing Gaussian distribution was performed using independent *t*-test or Analysis of Covariance (ANCOVA). Mann-Whitney *U* test was employed for variables showing non-Gaussian distribution. Categorical variables were compared by chi-square test. To test whether MRI parameters can distinguish MSA patients from control subjects, we performed binary logistic regression analyses. In addition, area under the curve values (AUCs) of receiver operating characteristic (ROC) curves obtained from each binary logistic regression model underwent pairwise comparison. Corrections for multiple testing were completed with the Bonferroni procedure. Statistical analyses were executed by SPSS 18.0 (SPSS Inc, Chicago, IL, USA) and MedCalc 18.6 (MedCalc Software, Ostend, Belgium). Statistical significance was defined as $p < 0.05$.

3. Results

The demographic and imaging characteristics of the enrolled subjects are summarized in Table 1. There were no significant differences in age and gender ratio between the MSA-total and control subjects. The MSA-P group had more female subjects (M:F 8:17) compared to the control group (13:9, chi-square test, corrected $p = 0.024$). Age, gender ratio, disease duration and H&Y stage did not show significant differences between the MSA-P and −C patients. However, the MSA-P patients had significantly higher UPDRS and UMSARS scores than the MSA-C subjects (Table 1).

MSA-total subjects had significantly higher putaminal MD and R2* values, and smaller volumes than the control subjects on average. Similarly, the MSA-P patients showed higher MD and R2* values, and smaller volumes compared to the MSA-C and control subjects. There was no significant difference in R2* values between MSA-C and control subjects (Table 1). In the binary logistic regression analyses, 3 putaminal MRI parameters were significant to discriminate the MSA-total group from the control subjects (Supplementary Material 2). However, when ROC curves from each binary logistic regression model were compared, the AUC values obtained by the predictive probability of the R2* values (0.719) was significantly lower than those for volume (AUC = 0.903; pairwise comparison with AUC of R2*, corrected $p < 0.001$), or MD values (AUC = 0.861; pairwise comparison with AUC of R2*, corrected $p = 0.013$) (Fig. 1; Supplementary Material 3).

In the linear regression analyses covariated with age, gender and disease duration, R2* values were correlated with volume (standardized beta = −0.603, corrected $p < 0.001$) and MD values (standardized beta = 0.619, corrected $p < 0.001$) in the putamen of the MSA-total patients. When locally estimated scatterplot smoothing (LOESS) was applied, associations between R2* with volume and MD values showed a non-linear pattern such as exponential (R2* values and volume) or quadratic (R2* and MD values) (Supplementary Material 4).

Table 1
Demographics and putaminal MRI parameters of enrolled subjects.

	MSA-total	MSA-P	MSA-C	Control	MSA-total *vs.* control (*p*)	MSA-P *vs.* MSA-C (*p*)	MSA-P *vs.* control (*p*)	MSA-C *vs.* control (*p*)
Age	59.1 ± 7.0	59.5 ± 7.5	58.2 ± 6.0	60.3 ± 6.3	0.505[a]	0.573[e]	0.495 [e]	0.287 [e]
Gender (M:F)	14:25	8:17	6:8	13:9	0.080[b]	0.461[b]	0.012 [b*]	0.228 [b]
Disease duration	26.6 ± 12.7	27.4 ± 12.5	25.1 ± 13.1	–		0.334[e]		
UPDRS-III	34.0 ± 11.7	38.3 ± 10.9	26.4 ± 9.0	–		< 0.001[e*]		
UMSARS-II	22.0 ± 5.4	23.6 ± 5.3	18.9 ± 4.1	–		< 0.001[a*]		
H&Y	3.0 ± 0.6	3.1 ± 0.6	2.9 ± 0.5	–		0.157[e]		
MMSE	25.5 ± 2.9	25.5 ± 2.8	25.6 ± 2.9	27.6 ± 1.8	0.008[e*]	0.983 [e]	0.010[e*]	0.061[e]
MRI parameters								
R2*	27.62 ± 6.82	29.57 ± 7.69	24.12 ± 2.40	24.8 ± 3.2	0.002[c*]	0.001[c*]	< 0.001 [c*]	0.761 [c]
MD (× 10^{-4})	8.11 ± 0.84	8.36 ± 0.88	7.64 ± 0.49	7.30 ± 0.33	< 0.001[c*]	< 0.001 [c*]	< 0.001 [c*]	< 0.001 [c*]
Volume	3976.57 ± 993.31	3575.01 ± 841.99	4693.64 ± 833.88	5354.83 ± 636.94	< 0.001[d*]	< 0.001[d*]	< 0.001[d*]	< 0.001[d*]

Mean ± SD; Disease duration = months; UPDRS-III = Unified Parkinson's Disease Rating Scale, part III; UMSARS = Unified Multiple System Atrophy Rating Scale; H&Y = Hoehn & Yahr stage; MMSE = Mini-mental state examination; MD = Mean diffusivity; a = independent *t*-test; b = chi-square test; c = Analysis of Covariance (ANCOVA) test, covariated with age and gender; d = ANCOVA test, covariated age, gender and total intracranial volume; e = Mann-Whitney *U* test; * = statistically significant after correction for multiple testing.

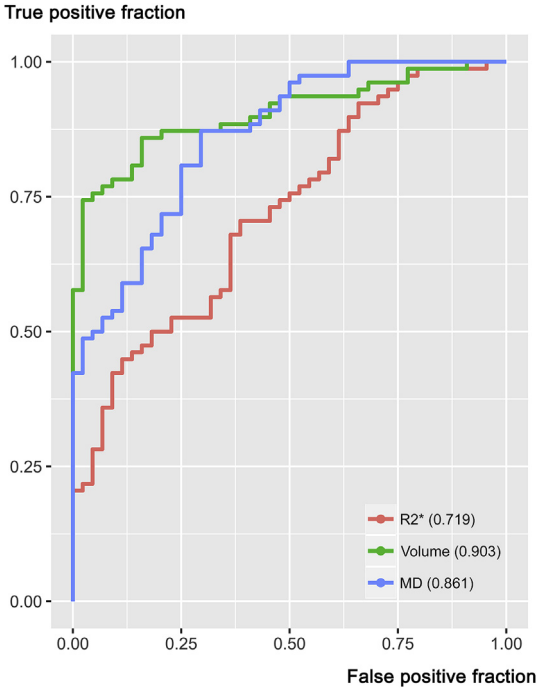

Fig. 1. Receiver Operating Characteristics (ROC) curves for MRI parameters discriminating between MSA and control putamen. Numbers in parentheses = Area Under Curve (AUC); MD = mean diffusivity.

Comparisons between CPs of MRI parameter changes in total MSA patients revealed that the CPs of R2* increments without volume atrophy or MD increments were significantly lower than the opposite cases (i.e. CPs of putaminal atrophy without R2* increment), regardless of cut-off values. CPs of volume atrophy without MD increments were higher than those of MD increments without volume atrophy. After correction for multiple testing, these results were significant only when the cut-off value was applied as 2.0 SD away from the mean values of the control subjects (Fig. 2 and Table 2). In MSA-P patients, CPs of R2* increment without volume atrophy were significantly lower than the opposite cases. CPs of R2* increment without MD increment were also lower than MD increment without R2* increment, however, the differences were statistically significant when cut-off value was defined as 1.5 SD. In MSA-C patients, CPs of MRI changes showed similar trends (nominal $p < 0.1$), however, none of CP comparisons did reach the statistical significance after correction for multiple testing (Supplementary Material 5 and 6).

4. Discussion

We applied the CP method in this study to predict the temporal order of multimodal MRI changes in MSA patients, and found significantly lower CPs for putaminal R2* increments without volume contractions or MD increments than for the opposite cases. There were similar trends when patients were divided into MSA-P and C subgroups. Our findings suggest that R2* increments can be mostly observed under volume contractions or MD increments. This would have resulted in the lower diagnostic ability of the R2* values in our study than for volume and MD values to discriminate MSA patients from control subjects.

In previous reports, MD values or volume were highly sensitive in detecting neurodegenerative changes in earlier disease stages [12,13]. Rising increments in R2* values in the putamen of MSA patients was significantly associated with atrophy [3]. Similarly, R2* values in the substantia nigra of patients with Parkinson's disease (PD) were significantly increased in the mid-stage and late-stage, but not early stage, whereas DTI changes were significant in all stages [14]. Taken together, these findings suggest that iron deposition detected by iron-sensitive MRI in the putamen of MSA patients might occur with advancing disease and follow microstructural DTI and atrophic changes.

The accumulation of non-heme iron in oligodendroglia, microglia, as well as neurons and astrocytes is believed to accelerate neurodegenerative processes [15,16]. A longitudinal MRI study in healthy older adults showed that higher iron-related signal in the putamen was predictive for faster declines in volume [17]. We observed non-linear, exponential (or quadratic) associations between R2* and volume (or MD values). The detrimental effect of excess iron accumulation on neuronal viability may become more pronounced with the progression of neurodegeneration and excessive iron may serve as an impending marker for accelerated neurodegeneration. Therefore, the removal of such iron may slow down a secondary progression caused by iron accumulation and associated toxicity.

It has been hypothesized that concomitant iron accumulation, oxidative stress, and neuroinflammation play a crucial role in the neurodegeneration associated with MSA [16,18]. Iron accumulation can induce oxidative stress and microglial activation, promoting α-synuclein aggregation [16]. In addition, impaired iron homeostasis can lead to the abnormal redistribution of iron. An increase in ferritin iron coupled with a reduction in ferroportin expression has been detected in the pons and putamen, suggesting a potential deficit in bioavailable iron despite an excess of tissue iron [19]. In oligodendrocytes, such iron dysregulation may cause energy and lipid metabolism dysfunctions, as well as further myelin dysfunction [20,21]. The maldistribution of iron could be treated by a conservative strategy of chelation based on iron scavenging and its redistribution to areas of iron deficiency [22]. Such

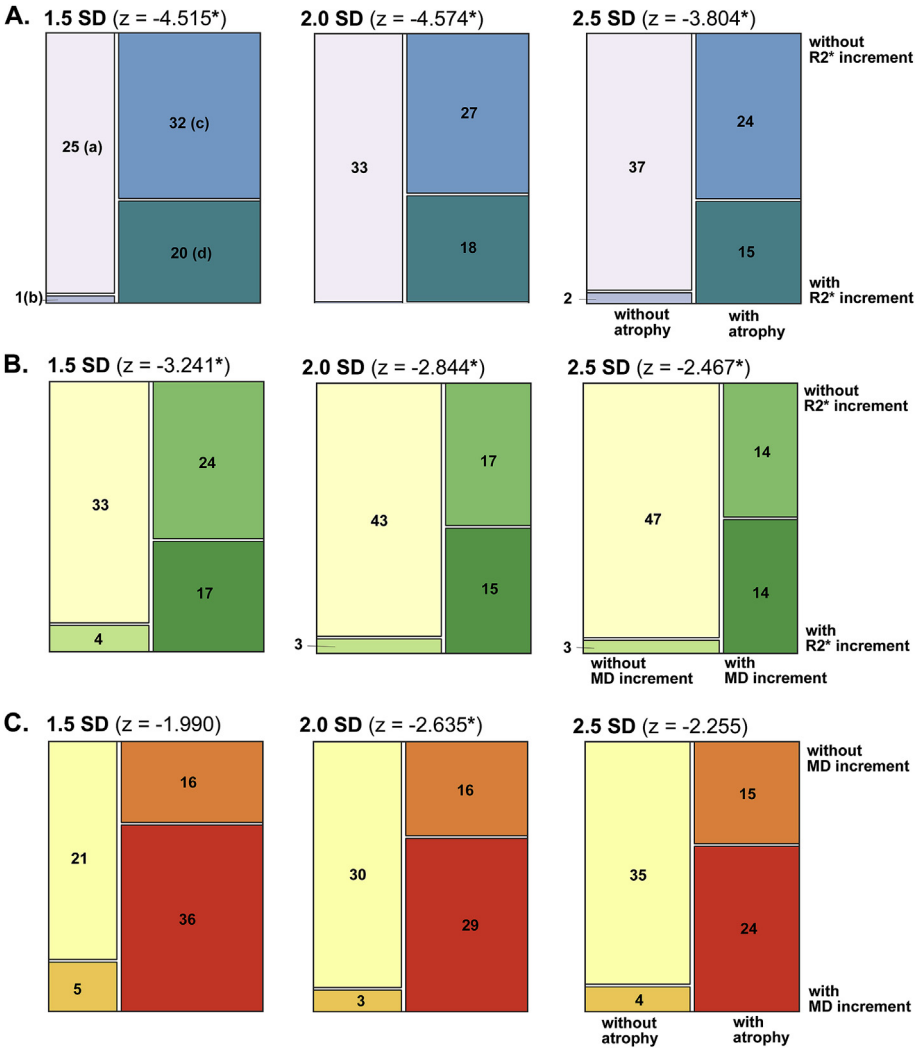

Fig. 2. Mosaic plots showing the presence/absence of R2* increment and atrophy (A), R2* and MD increment (B), and MD increment and atrophy (C) in MSA patients. 1.5, 2.0 or 2.5 SD represent cut-off values (e.g. 1.5 SD: using a cut-off value of 1.5 SD from the mean values of control subjects). Numbers in boxes = numbers of putamen; z scores = comparison of conditional probability [b/(a+b)] and [c/(a+c)]; * = statistically significant after Bonferroni correction.

Table 2
Comparison between conditional probabilities of MRI parameter changes.

Cut-off values†	CP: R(+)A(−)	CP: A(+)R(−)	z	*p*
1.5 SD	0.038	0.561	−4.515	< 0.001*
2.0 SD	0.000	0.450	−4.574	< 0.001*
2.5 SD	0.051	0.393	−3.804	< 0.001*
	CP: R(+)M(−)	**CP: M(+)R(−)**		
1.5 SD	0.108	0.421	−3.241	0.001*
2.0 SD	0.065	0.283	−2.845	0.004*
2.5 SD	0.060	0.230	−2.467	0.014*
	CP: M(+)A(−)	**CP: A(+)M(−)**		
1.5 SD	0.192	0.432	−1.990	0.047
2.0 SD	0.091	0.348	−2.635	0.008*
2.5 SD	0.103	0.300	−2.255	0.024

† = cut-off values were defined as 1.5, 2.0 or 2.5 SD away from mean values of control subjects; CP: conditional probability; R = R2* increment; A = volume atrophy; M = MD increment; (+) = presence of MRI parameter change; (−) = absence of MRI parameter change; z = z-statistics of comparison of 2 CPs; *p* = calculated from z-statistics, uncorrected for multiple comparison; * = statistically significant after correction for multiple testing.

therapeutic strategies have been proposed to modify the disease course of MSA [16].

Recently, iron targeting therapy using deferiprone has been applied to PD [22]. Deferiprone treatment reduces iron content measured by quantitative MRI and is associated with a trend toward improvement in motor scales [23,24]. In MSA, the excessively deposited iron in the putamen may be a putative target of chelation therapy. However, the heterogeneity of iron content over the course of neurodegenerative changes can cause challenges for selecting patients and evaluating efficacy.

We note several limitations in the present study. First, the sample size was small and the cases in the study were not pathologically proven. Second, as mentioned above, our results were based on the hypothesis that the preceding pathological changes might have a higher severity. Thus, the present study should be considered exploratory in nature, and a cross-validation study with a longitudinal design is required. If there were no significant differences in the longitudinal change rates of the MRI parameters, a proceeding change in neuroimaging would show larger differences in a greater number of subjects [8]. Previous neuroimaging studies investigating longitudinal changes of MRI parameters in MSA patients demonstrated similar annual change rates for R2* (about 7%/year), MD (about 9%/year), and volume (4%/year) [3,12]. Therefore, the CP method may be suitable for predicting

the temporal order of multimodal MRI changes. Finally, there were no significant differences in R2* values between MSA-C and control subjects. This can be attributed to the short duration of the disease. MSA-C patients exhibited slower progression of atrophy in the putamen than MSA-P subjects [3].

In summary, our findings suggest that iron-related signal changes in MRI scans might occur after volume atrophy or DTI changes. It is possible that putaminal iron accumulation may be a secondary phenomenon resulting from neurodegeneration or neuroinflammation during MSA. A further longitudinal study investigating the effect of iron deposition on putaminal degeneration is required.

Conflicts of interest

The authors have nothing to disclose.

Acknowledgements

This research was supported by Basic Science Research Program through the National Research Foundation of Korea (NRF) funded by the Ministry of Education, Science and Technology (2014R1A1A2059252) and the Korea Health Technology R&D Project through the Korea Health Industry Development Institute (KHIDI) funded by the Ministry of Health and Welfare (grant number: HI18C0713).

Appendix A. Supplementary data

Supplementary data to this article can be found online at https://doi.org/10.1016/j.parkreldis.2019.02.030.

References

[1] J.H. Lee, Y.H. Han, B.M. Kang, C.W. Mun, S.J. Lee, S.K. Baik, Quantitative assessment of subcortical atrophy and iron content in progressive supranuclear palsy and parkinsonian variant of multiple system atrophy, J. Neurol. 260 (2013) 2094–2101.
[2] G. Barbagallo, M. Sierra-Pena, F. Nemmi, A.P. Traon, W.G. Meissner, O. Rascol, et al., Multimodal MRI assessment of nigro-striatal pathway in multiple system atrophy and Parkinson disease, Mov. Disord. 31 (2016) 325–334.
[3] J.H. Lee, T.H. Kim, C.W. Mun, T.H. Kim, Y.H. Han, Progression of subcortical atrophy and iron deposition in multiple system atrophy: a comparison between clinical subtypes, J. Neurol. 262 (2015) 1876–1882.
[4] J.B. Schulz, T. Klockgether, D. Petersen, M. Jauch, W. Muller-Schauenburg, S. Spieker, et al., Multiple system atrophy: natural history, MRI morphology, and dopamine receptor imaging with 123IBZM-SPECT, J. Neurol. Neurosurg. Psychiat. 57 (1994) 1047–1056.
[5] M.J. Lee, T.H. Kim, C.W. Mun, H.K. Shin, J. Son, J.H. Lee, Spatial correlation and segregation of multimodal MRI abnormalities in multiple system atrophy, J. Neurol. 265 (2018) 1540–1547.
[6] G.K. Wenning, F. Geser, F. Krismer, K. Seppi, S. Duerr, S. Boesch, et al., The natural history of multiple system atrophy: a prospective European cohort study, Lancet Neurol. 12 (2013) 264–274.
[7] K.A. Josephs, M.E. Murray, J.L. Whitwell, N. Tosakulwong, S.D. Weigand, L. Petrucelli, et al., Updated TDP-43 in Alzheimer's disease staging scheme, Acta Neuropathol. 131 (2016) 571–585.
[8] H. Cho, J.Y. Choi, M.S. Hwang, Y.J. Kim, H.M. Lee, H.S. Lee, et al., In vivo cortical spreading pattern of tau and amyloid in the Alzheimer disease spectrum, Ann. Neurol. 80 (2016) 247–258.
[9] H. Cho, H.S. Lee, J.Y. Choi, J.H. Lee, Y.H. Ryu, M.S. Lee, et al., Predicted sequence of cortical tau and amyloid-beta deposition in Alzheimer disease spectrum, Neurobiol. Aging 68 (2018) 76–84.
[10] S. Gilman, G.K. Wenning, P.A. Low, D.J. Brooks, C.J. Mathias, J.Q. Trojanowski, et al., Second consensus statement on the diagnosis of multiple system atrophy, Neurology 71 (2008) 670–676.
[11] I. Hwang, C.H. Sohn, K.M. Kang, B.S. Jeon, H.J. Kim, S.H. Choi, et al., Differentiation of parkinsonism-predominant multiple system Atrophy from idiopathic Parkinson disease using 3T susceptibility-weighted MR imaging, focusing on putaminal change and lesion asymmetry, AJNR (Am. J. Neuroradiol.) 36 (2015) 2227–2234.
[12] M.T. Pellecchia, P. Barone, C. Vicidomini, C. Mollica, E. Salvatore, M. Ianniciello, et al., Progression of striatal and extrastriatal degeneration in multiple system atrophy: a longitudinal diffusion-weighted MR study, Mov. Disord. 26 (2011) 1303–1309.
[13] C. Brenneis, K. Egger, C. Scherfler, K. Seppi, M. Schocke, W. Poewe, et al., Progression of brain atrophy in multiple system atrophy. A longitudinal VBM study, J. Neurol. 254 (2007) 191–196.
[14] G. Du, M.M. Lewis, S. Sen, J. Wang, M.L. Shaffer, M. Styner, et al., Imaging nigral pathology and clinical progression in Parkinson's disease, Mov. Disord. 27 (2012) 1636–1643.
[15] D.W. Dickson, W. Lin, W.K. Liu, S.H. Yen, Multiple system atrophy: a sporadic synucleinopathy, Brain Pathol. 9 (1999) 721–732.
[16] C. Kaindlstorfer, K.A. Jellinger, S. Eschlbock, N. Stefanova, G. Weiss, G.K. Wenning, The relevance of iron in the pathogenesis of multiple system Atrophy: a viewpoint, J. Alzheimers Dis. 61 (2018) 1253–1273.
[17] A.M. Daugherty, N. Raz, Accumulation of iron in the putamen predicts its shrinkage in healthy older adults: a multi-occasion longitudinal study, Neuroimage 128 (2016) 11–20.
[18] E. Valera, E. Masliah, The neuropathology of multiple system atrophy and its therapeutic implications, Auton. Neurosci. 211 (2018) 1–6.
[19] N.P. Visanji, J.F. Collingwood, M.E. Finnegan, A. Tandon, E. House, L.N. Hazrati, Iron deficiency in parkinsonism: region-specific iron dysregulation in Parkinson's disease and multiple system atrophy, J. Parkinson's Dis. 3 (2013) 523–537.
[20] B. Todorich, J.M. Pasquini, C.I. Garcia, P.M. Paez, J.R. Connor, Oligodendrocytes and myelination: the role of iron, Glia 57 (2009) 467–478.
[21] J.H. Wong, G.M. Halliday, W.S. Kim, Exploring myelin dysfunction in multiple system atrophy, Exp. Neurobiol. 23 (2014) 337–344.
[22] C. Moreau, J.A. Duce, O. Rascol, J.C. Devedjian, D. Berg, D. Dexter, et al., Iron as a therapeutic target for Parkinson's disease, Mov. Disord. 33 (2018) 568–574.
[23] D. Devos, C. Moreau, J.C. Devedjian, J. Kluza, M. Petrault, C. Laloux, et al., Targeting chelatable iron as a therapeutic modality in Parkinson's disease, Antioxidants Redox Signal. 21 (2014) 195–210.
[24] A. Martin-Bastida, R.J. Ward, R. Newbould, P. Piccini, D. Sharp, C. Kabba, et al., Brain iron chelation by deferiprone in a phase 2 randomised double-blinded placebo controlled clinical trial in Parkinson's disease, Sci. Rep. 7 (2017) 1398.